

# The Curvature – Energy Relations in Buckling Analysis of Tubular Wind Turbine Towers

Ma, Yang; Martinez-vazquez, Pedro; Baniotopoulos, Charalampos

DOI:

[10.1002/cepa.1802](https://doi.org/10.1002/cepa.1802)

License:

Creative Commons: Attribution-NonCommercial-NoDerivs (CC BY-NC-ND)

*Document Version*

Publisher's PDF, also known as Version of record

*Citation for published version (Harvard):*

Ma, Y, Martinez-vazquez, P & Baniotopoulos, C 2022, 'The Curvature – Energy Relations in Buckling Analysis of Tubular Wind Turbine Towers', *ce/papers*, vol. 5, no. 4, pp. 643-652. <https://doi.org/10.1002/cepa.1802>

[Link to publication on Research at Birmingham portal](#)

## General rights

Unless a licence is specified above, all rights (including copyright and moral rights) in this document are retained by the authors and/or the copyright holders. The express permission of the copyright holder must be obtained for any use of this material other than for purposes permitted by law.

- Users may freely distribute the URL that is used to identify this publication.
- Users may download and/or print one copy of the publication from the University of Birmingham research portal for the purpose of private study or non-commercial research.
- User may use extracts from the document in line with the concept of 'fair dealing' under the Copyright, Designs and Patents Act 1988 (?)
- Users may not further distribute the material nor use it for the purposes of commercial gain.

Where a licence is displayed above, please note the terms and conditions of the licence govern your use of this document.

When citing, please reference the published version.

## Take down policy

While the University of Birmingham exercises care and attention in making items available there are rare occasions when an item has been uploaded in error or has been deemed to be commercially or otherwise sensitive.

If you believe that this is the case for this document, please contact [UBIRA@lists.bham.ac.uk](mailto:UBIRA@lists.bham.ac.uk) providing details and we will remove access to the work immediately and investigate.

## ORIGINAL ARTICLE



**SDSS 2022**  
The International Colloquium on Stability  
and Ductility of Steel Structures  
14-16 September, University of Aveiro, Portugal



Ernst & Sohn  
A Wiley Brand

# The Curvature – Energy Relations in Buckling Analysis of Tubular Wind Turbine Towers

Yang Ma<sup>1</sup>, Pedro Martinez-Vazquez<sup>1</sup>, Charalampos Baniotopoulos<sup>1</sup>

## Correspondence

Prof. Charalampos Baniotopoulos  
Department of Civil Engineering,  
School of Engineering  
University of Birmingham  
Birmingham, UK  
Email: c.baniotopoulos@bham.ac.uk

## Abstract

A former study on wind turbine tower collapse incidences throughout the past 40 years revealed that among the various types the buckling failure was the most catastrophic as led to collapse of tubular tower shell structures. As the modern harvesting of wind energy is usually performed by wind turbine towers being cylindrical shells of thin walls, the need of thorough investigation of the buckling behaviour of shell structures operating under extreme environmental actions is obvious. The present paper addresses such knowledge gap through the study of a series of 100 numerical models underpinned by the well-established Riks Method for buckling analysis. The method enables the scrutiny of tower shell elements under axial load and bending moment. Within the proposed framework of curvature–energy analysis, the energy stored within an imperfect shell structure is expressed and quantified through cross-section diaphragms and symbolic lines, covering pre-buckling, transient stage, and post-buckling performance close to the bifurcation point. The analysis unveils changes of local surface curvature and energy flows with multiple longitudinal and circumferential wavenumbers taking place during the pre-buckling process. Wavenumbers and curvature changes induce the energy magnitude jumping over to the adjacent buckling eigenmodes. Furthermore, the mode jumping sees a faster and more convergence result with higher bending moments. The diversity of the final buckling mode largely determined by the variance of shell geometry, compression–bending ratio and boundary conditions.

## Keywords

Shell structure, Buckling, Riks Method, Curvature, Energy method

## 1 Introduction

The high demand for wind energy requires optimised productivity from wind power plants fuelled by technological improvements. This inserts in a production chain that is not exempt from errors or omissions, as discussed in previous studies [1]. The most common reasons for wind turbine tower collapses relates to extreme wind hence careful consideration has to be made when quantifying this type of loading. Derived from such critical conditions, researchers have identified buckling types affecting the tower shell components across its circumference and length. In mathematical terms this could be explained in terms of wavenumbers that set at specific ranges.

The buckling phenomenon remains to be fully understood. While there is consensus on the fact that torsional and shear effects are negligible in comparison with axial effects [1-5], knowledge gaps still reflect on discrepancies between theoretical and experimental studies. That is one of the causes for which a perfect shell section for wind turbine towers has not been determined. At the microscale

imperfections are usually found on the surface of steel shells. This is relevant as such initial imperfections are determinant of how buckling develops [4, 6-11]. This and other aspects of performance have been highlighted through experimental work undertaken on cylindrical shell structures, often building upon a comprehensive shell-buckling experiment carried out by NASA in the 1960s [12]. In that study, the following regression model for the lower bound was put forward,  $\alpha$  represents the knock-down factor based on the theoretical ideal buckling capacity:

$$\alpha = 1 - 0.901(1 - e^{-\sqrt{(R/t)/16}}) \quad (1)$$

Von Karman [13] first introduced the curvature issue as a controlling parameter of shell buckling. That work already highlighted discrepancies between laboratory tests and classical buckling theory. Following, Koiter [14] (English version available from 1967) identified buckling load threshold in relation to stability and added explanations around differences between test results and theoretical values. They accepted wall imperfections on cylindrical shells as a key factor to unchain instability [15,16]. Other experimental studies identified boundary conditions, load

1. University of Birmingham, Birmingham, UK.

alignment, and material non-linearities, as sources of analytical error [17-19].

In Eq. (1) the radius to thickness ratio ( $R/t$ ) relates to the curvature of cylinder shells. In the literature we find the Gaussian curvature,  $K$ , as a practical expression that intervenes the imperfection parameter. If  $K$  is positive, the shell shape is typically spherical or arced, and sensitive to imperfection when loaded, especially external pressures [20-23]. When  $K$  is negative, the shell surface adopts an inward form, which is not significantly sensitive to initial imperfections on its surface [24]. Wu [25] has studied negative Gaussian curvature in steel and hyperbolic cooling towers. Their studies report that  $K$  equal to zero locates the structure in the interval between sensitive spherical and the insensitive inward shell prone to undergo complex sensitive behaviour related to imperfections [9, 10, 16, 26]. Furthermore, Khamlichi [27] investigated localised axisymmetric imperfections and revisited the analytical solutions (shell equations) by Von Karman-Donnell. They concluded that the buckling load could be up to twofold lower than that indicated by the general defects.

## 2 Curvature Analysis and Energy Methods on Buckling Analysis

Energy methods applied to buckling can be traced to Von Karman and Tsien [28], who further developed equations of nonlinear buckling after Donnell [29]. Energy methods consider multiple equivalent buckling paths near the bifurcation point, through a series of unstable equations. The well-known Ritz energy method enables nonlinear elastic buckling analysis of cylindrical shells under compression loads while permits mode-jumping performances as experimentally observed in postbuckling stages [30]. Recently, the authors simplified the framework of energy methods for buckling analysis of wind turbine towers under combined loads [31], and this research lays out extended work.

More generally, if there exists the horizontal strain term  $\epsilon_y$ , a general form of local curvature  $K$  would be:

$$K = -\frac{\partial^2 \epsilon_y}{\partial x^2} + \frac{\partial^2 \gamma_{xy}}{\partial x \partial y} - \frac{\partial^2 \epsilon_x}{\partial y^2} \quad (2)$$

In the case of wind turbine towers, the Gaussian curvature of cylindrical shell is equal to zero, thus, the local curvature is equal to zero at any point on the shell, if buckling fails to occur, whether local buckling or overall buckling, then this can be expressed as:

$$\frac{\partial^2 \epsilon_y}{\partial x^2} - \frac{\partial^2 \gamma_{xy}}{\partial x \partial y} + \frac{\partial^2 \epsilon_x}{\partial y^2} = 0 \quad (3)$$

This equilibrium, referred to as plane-strain compatibility condition, provides us with a criterion to determine whether buckling has taken place. After shell buckling develops, changes in the local Gaussian curvature can be written as:

$$\frac{\partial^2 \epsilon_y}{\partial x^2} - \frac{\partial^2 \gamma_{xy}}{\partial x \partial y} + \frac{\partial^2 \epsilon_x}{\partial y^2} = \Delta K_i \quad (4)$$

Furthermore, the local Gaussian curvature can be expressed in terms of the principal radii of curvature  $R_1 R_2$  according to principal directions  $X$  and  $Y$ , as in [32]:

$$K = \frac{1}{R_1 R_2} \quad (5)$$

while the Cartesian coordinate interconnection could be written as:

$$Z = (X^2/2R_1) + (Y^2/2R_2) \quad (6)$$

In these equations,  $\kappa_1, \kappa_2$  represent the change of curvature in the principal directions  $X, Y$ , namely, 1, 2, at a certain local point. The differential on Equation (5) would then provide the change of local curvature  $\Delta K_i$  as follows:

$$\Delta K_i = \frac{\kappa_1}{R_2} + \frac{\kappa_2}{R_1} = -\frac{\partial^2 \epsilon_y}{\partial x^2} + \frac{\partial^2 \gamma_{xy}}{\partial x \partial y} - \frac{\partial^2 \epsilon_x}{\partial y^2} \quad (7)$$

Equation (7) as it establishes a relationship between displacements and curvature changes, becomes the foundation for the estimation of membrane effects [33, 34].

According to this, it is possible to revisit the initial circumferential displacement of the shell surface, to be expressed as:

$$f = -C_0 \sin \frac{n\pi x}{L} + a\zeta \cos 2\theta \quad (8)$$

where,  $n$  is half-wavenumber,  $\zeta$  is dimensionless length,  $L$  is the length of cylindrical shell, and  $a$  and  $C_0$  are constant parameters. While this function highlights a relation between shell length and radial displacement, should be periodic throughout the circumference hence prone to be modelled through trigonometric functions.

By considering the well-developed manufacturing performance for modern wind turbine towers, the axisymmetric imperfection type is found regularly due to the steel shell is made by revolution, although another type of imperfection, asymmetric shape, is more frequently observed on-site owing to transportation and installation. The shape change (namely the curvature change) brought about by imperfection in a perfect shell reduces the membrane action significantly, while the membrane part plays a dominant role in shell-stress carryings. Imperfection sensitivity relates to membrane effect on initial post-buckling behaviour for cylindrical shells, as curvature changes affect the pre-buckling path that principally determines post-buckling behaviour [16, 33]. It is explained in EN 1993-1-6 that when the imperfection amplitude is less than 10% from the perfect shape, the verification should be done particularly due to the small imperfection ratio does not yield a lower value for the reduction ratio in GMNIA. It could be observed from the review by Teng and Rotter of the four experiment results, that for the axisymmetric imperfection, the buckling stress drops dramatically half of the entire asymptote amount in the first 10 % of the imperfection amplitude followed by another half in the next 90 %  $w_0/t$  [34]. As the imperfection is rarely large in modern wind turbine industry, and according to the geometrical imperfection tolerance by design codes, 0.1 of the first axisymmetric eigenmode in the dimension of shell thickness for initial geometry imperfection is relatively appropriate and practical in this case. When considering the asymmetric imperfection, such as the second modal shape and third modal shape, this research referred to the review by Teng and Rotter [34] about the non-symmetric buckling to the imperfect shells showing that the asymmetric imperfection amplitude in the range of -0.05 to 0.05 reveals the most noticeable variations. Therefore, 5% for the second modal shape and 2.5% for the third modal shape have been selected in this research for obtaining the lower value of buckling capacity [31]. In total, this setting introduces a superposition imperfection at 17.5 % according to the dimension of shell wall thickness and this figure falls into the range between the minimum 10 % by EN 1993-1-6 and the maximum tolerance 40 %. These insensitive modal shapes after the third eigenvalue are neglected in the following FEM analysis. Geometrical imperfections are estimated with a combination of eigenvalues weighed with amplitude parameters. The dimensionless amplitude parameter  $w_0/t$  were fixed to 0.1, 0.05, and 0.025, respectively for the target eigenvalues, where  $w_0$  is the

amplitude of initial geometric imperfection. This combination has been found reliable for the study of wind turbine towers, especially in the extreme-case scenarios when wind power plants operate [1, 31]. Based on this, a sinusoidal shape function  $f_0$  can be used to deform the perfect shell based on the eigenvalues referred above:

$$f_0 = 0.1 \sin\left(\frac{\pi x}{l_1}\right) \sin\left(\frac{\pi y}{b_1}\right) + 0.05 \sin\left(\frac{\pi x}{l_2}\right) \sin\left(\frac{\pi y}{b_2}\right) + 0.025 \sin\left(\frac{\pi x}{l_3}\right) \sin\left(\frac{\pi y}{b_3}\right) \quad (9)$$

In Eq. (9),  $l_1, b_1$  derive from the first eigenvalue while  $l_2, b_2, l_3$  and  $b_3$  are derived from the second and third eigenvalues, respectively.

Before now based on energy methods, the total internal strain energy equals the sum of strain energies due to axial compression and bending, which is represented as:

$$\begin{aligned} \delta U &= \delta U(\text{axial compression}) + \delta U(\text{bending}) \\ &= \delta[U_b + U_m](\text{axial compression}) \\ &\quad + \delta U[U_b + U_m](\text{bending}) \end{aligned} \quad (10)$$

The two strain energy components use the same approximation to determine curvature and mid-surface deformation, which are consistent with continuity conditions for a cylindrical shell section.

### 3 Modelling Details and Assumptions in Finite Element Analysis

In this investigation we target the secondary bottom which is the part most vulnerable to buckling failure. For the secondary bottom section, especially for a cylindrical shell structure under combined loads, a pure shell section is the best choice for a buckling mechanism investigation due to the variations of stiffening configurations that can influence the buckling behaviour comprehensively. In terms of tower geometry, the buckling behaviour of a pure cylindrical shell section depends on diameter, wall thickness, and cylinder length, hence in this study we use the ratios between these geometry configurations to parametrically analyse the failure process. It is widely accepted that the spatial extent of shell geometry has no relation to buckling behaviour i.e., shells of different proportion but with the same L/R and R/t ratios exhibit the same buckling responses [16, 23, 29, 31, 34, 35].

Modern cylindrical steel towers used for wind energy harvesting comprise numerous prototypes being the NREL 5 MW baseline wind turbine the most widely adopted for manufacture, hence for the FEM presented here [36]. Table 1 provides details of the adopted prototype. The diameter of the tower is fixed to 6.0 m while its wall thicknesses changes in 3 mm increments, overall ranging between 24 mm and 36 mm. Shell lengths are 9.0 m, 12.0 m, 15.0 m and 20.0 m, with the ratios L/R and R/t ratios listed in the table.

**Table 1** Model geometry size adopted for the FEM analysis

No.	Diameter D	Length L	Thickness t	L/R	R/t
1	6000	20,000	24	6.66	125
2	6000	15,000	24	5	125
3	6000	12,000	24	4	125
4	6000	9000	24	3	125

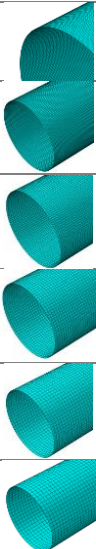
5	6000	20,000	27	6.66	111.11
6	6000	15,000	27	5	111.11
7	6000	12,000	27	4	111.11
8	6000	9000	27	3	111.11
9	6000	20,000	30	6.66	100
10	6000	15,000	30	5	100
11	6000	12,000	30	4	100
12	6000	9000	30	3	100
13	6000	20,000	33	6.66	90.91
14	6000	15,000	33	5	90.91
15	6000	12,000	33	4	90.91
16	6000	9000	33	3	90.91
17	6000	20,000	36	6.66	83.33
18	6000	15,000	36	5	83.33
19	6000	12,000	36	4	83.33
20	6000	9000	36	3	83.33

The parametric study is based on three load types: axial compression, bending, and combined bending and axial effects. The model geometries induced 100 shell prototypes that yield 20 linear buckling models and 80 specific load configurations. The boundary conditions applied to axial compression are, fixed support at the base but free to rotate and displace at the top edge. About bending and combined bending-axial effects, we restricted the horizontal displacement and rotations with respect to the x and y axis at the base keeping the top edge free to rotate and displace. Tie constraints applied along the circumferential directions according to a reference point at the centre of the edge circles simulating the action of flange and ring stiffeners.

Following the above, the S4R element [37] was chosen for ABAQUS buckling analysis using the Riks method, which controls force and displacement upon specification of the load proportionality factor (LPF). Linear elastic analyses yield linear eigenvalue which may suffice engineering purposes but is unable to reveal the post-buckling behaviour we were aiming for here. The Riks method is suitable for tracking post-buckling paths via a static analysis procedure, which reduces the calculation load for a dynamic analysis. The Riks increments implemented in ABAQUS thus approach the failure state until the fixed 1000 steps are completed, otherwise the job is aborted to prevent a lack of convergence. The thickness integration point was set to 7 and the maximum curvature control was 0.1, to provide additional post-buckling accuracy. The optimum mesh size shown in Table 2 that resulted from a mesh sensitivity test on 20 m length shell with 27 mm wall thickness. When the mesh size falls below 200mm, stress variations become meaningless, although the number of elements and nodes surge together with the CPU time and RAM occupation, which prevent the workstation to carry parallel calculations efficiently for handful of jobs filed up in ABAQUS. Hence a grid 200 mm × 200 mm was adopted for meshing each cylindrical shell

model. The elastoplastic parameterisation of material and stress-strain information correspond to S355 steel. This data constructed an 11-point curve characterised by a Poisson ratio of 0.3.

Table 2 Mesh sensitivity analysis results.

Mesh size (mm)	Von Mises Stress (MPa)	Max Principal Stress (MPa)	Arc Length (500th step)	Number of Elements	Meshing examples
50	437.35	502.53	0.042801	150,800	
100	437.34	502.44	0.042924	37,412	
150	437.31	502.27	0.043121	16,758	
200	437.02	502.01	0.043751	9,306	
250	434.72	498.77	0.045035	5,925	
300	428.10	486.95	0.157736	4,158	

The first step was to obtain the first three linear buckling eigenmodes for the models listed in Table 1. Classical theory predicts the first mode to be axisymmetric and the following two modes to be asymmetric. The initial imperfection discussed in previous sections was implemented in ABAQUS via keyword editing in GUI section. Figure 1 shows examples of the first three vibration modes of the shell section. Each segment is 20 m long and 30 mm thick as depicted in Figure 1. By combining the first three modes with the weighing coefficients of 10% (first mode), 5% (second mode), and 2.5% (third mode), we achieved the intended asymmetric initial geometry imperfection for each cylinder [14, 34]. It is to note that the first modal shape represented in the visualisation of ABAQUS is a function of surface displacement along the longitudinal direction, showing deviations from the original perfectly flat shell surface.

A section of the displacement curve, 35% of the length to the left end, has been selected for curve fitting. The best curve fitting results were carried out in MATLAB by using a function which transform a sine function to sine and cosine combinations. Figure 2 shows the fitted curve.

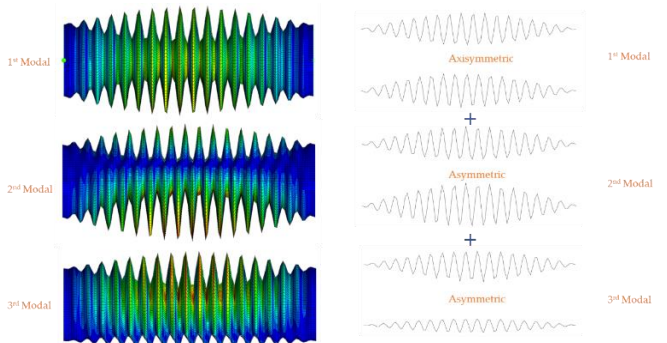


Figure 1 An illustration of the first three modes of the 20 m shell section at 30 mm thickness. The combination of modal shapes resulted in the asymmetric geometry imperfection.

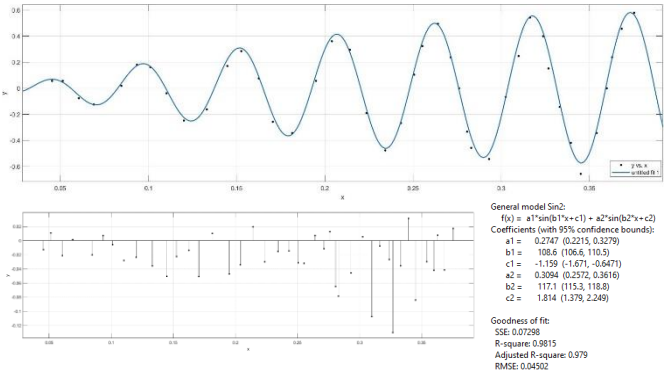


Figure 2 The curve fitting example by the sum of sinusoidal functions with two terms. The displacement function  $f(x)$  shares the convertible form; coefficients  $a_i, b_i$  were shown by the right side.

By substituting the coefficients depicted in Figure 2 in the equation systems reported in [31], we obtained a linear buckling load that enabled validation of results, as shown in Figure 3. With reasonable limits, the simulation showed consistency with theoretical results on different thickness cylinders. The discrepancy between theoretical and FEM results, in terms of both magnitude and shape, are attributed to the initial shape function adopted for the simulation. When we introduce the curve-fitted sinusoidal functions to the curve of the left 35% shell section, the phase diversifies leading to sine and inverted sine curves that switch trajectories. We reproduced the curve fitting function as  $f(x) = 0.2747 \sin(108.6x - 1.159) + 0.3094 \sin(117.1x + 1.814)$ . Meanwhile, the replaced initial shape function induced magnitude variances with respect to theoretical results, with discrepancies ranging between those obtained by using an ideal initial imperfect function and the curve fitting function. Along these lines, the magnitude of buckling load factors varied reasonably from 39.13% to 7.32% yet showing stable convergence. These results enabled to conclude that shape functions have a higher effect on shells with smaller wall thickness than on thicker shell surfaces.

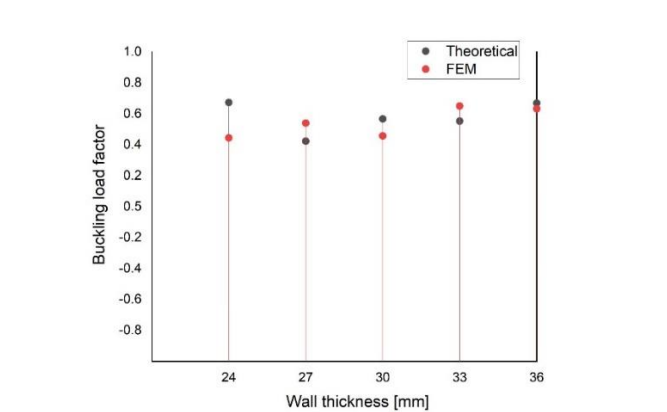


Figure 3 Linear buckling load in ABAQUS vs. buckling load using linear theory, in accordance with cylinders of various wall thickness.

## 4 Finite Element Results

### 4.1 Buckling Behaviour under Axial Compressions

The buckling behaviour of different segment lengths was compared using different L/R ratios. We compared the longest 20 m shell



section with the shortest 9 m models under axial compression on perfect shells. Buckling displacements generally vary. For example, the 9 m shell tends towards the 'elephant foot'-shaped at each end, while the 20 m shell has a one-sided asymmetric buckle point around the mid-length. On the other hand, it was found that the circumferential wavelength has less influence on the axial compression buckling, especially for longer cylinders [38]. Figure 4 shows how the longitudinal wavenumber changed along the extreme fibre on the compression side, which depicts local curvature evolution of the upper 2/3 of its length. The local curvature changed dramatically with the increase of the compression load: the wavenumber dropped in the early steps and maintained a long interval until the entire shell collapsed. In the meantime, circumferential curvature changes as illustrated in Figure 5.

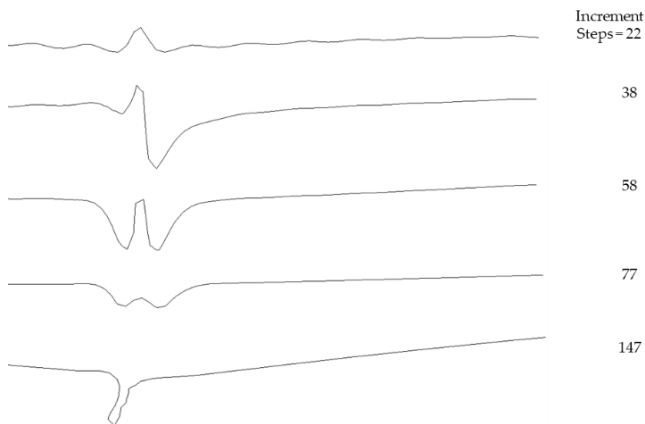


Figure 4 Shell (20 m at 24 mm) extreme fibre wavenumber change under axial compressive load.

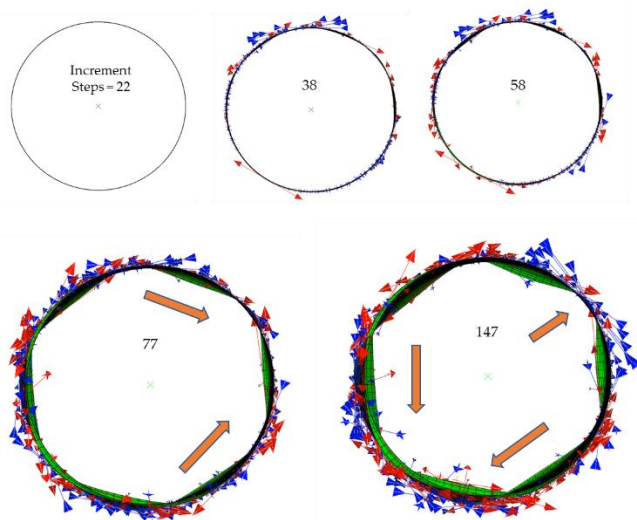


Figure 5 Shell (20 m at 24 mm) circumferential fibre curvature change under axial compressive load.

In Figure 5, blue arrows indicate inward curvature changes whereas red arrows represent outward curvature changes on the shell surface. The vectors indicate tendency of curvatures at each increment step. Moreover, the thick orange arrows follow the peak value of displacement i.e., the biggest deviation point. Those highlighted circumferential flow trends captured by the shape Equation (8), which changes with the angular coordinate  $\theta$ . Figure 6 shows how the circumferential curvature of the 9 m cylinder, remains less disturbed by the stress flow. The initial curvature presents an even distribution, although after few steps led to the 'elephant foot' type of bulge buckling near both ends.

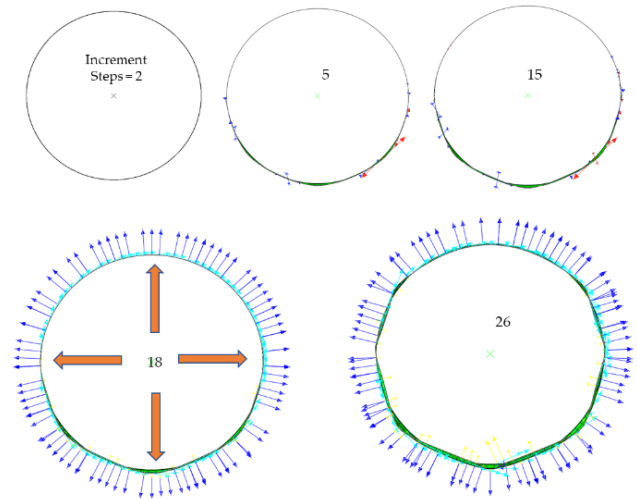


Figure 6 Shell (9 m at 24 mm) circumferential fibre curvature change under axial compressive load.

## 4.2 Buckling Behaviour under Bending

The main concern around pure bending effects in a wind turbine tower shell is the change of curvature, both longitudinal and circumferential. The distortion in the longitudinal direction would be expected to develop near the mid-span [8, 39] while the cross section undergoes the Brazier's effect of ovalisation [40]. These effects have been plotted for shell prototypes of 20 m long at 30 mm ( $L/R = 6.66$ ) and 9 m at 30 mm ( $L/R = 3$ ). The surface deformations and stress distributions are shown in Figure 7 and Figure 8.

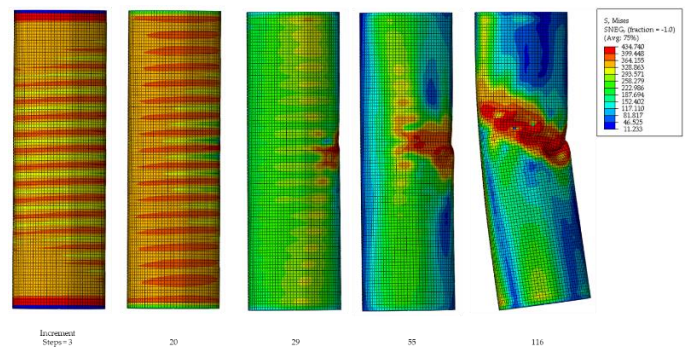


Figure 7 Shell (20 m at 30 mm) surface deformation and stress distribution under bending moment.

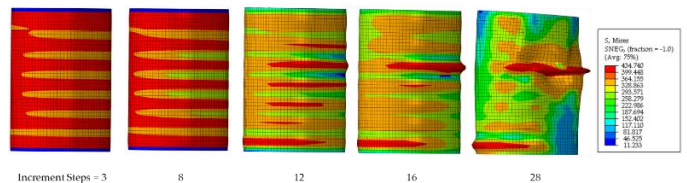


Figure 8 Shell (9 m at 30 mm) surface deformation and stress distribution under bending moment.

It is noticeable that both shell segments show buckle points locate near the mid-span on the compression side of the shell being the 9 m shell model more dependent on the boundary conditions as the secondary buckle point emerged on the bottom of opposite side. The stress arrangement along the shell surface has been affected, as it has less material length for energy dissipation. In the early stage of the pre-buckling process, wave-like displacements are observed along the shell length but concentrated rapidly at the mid-

span area, like a beam member. The cut-out view of the extreme fibre on the compression side on the 20 m shell model is illustrated in Figure 9.

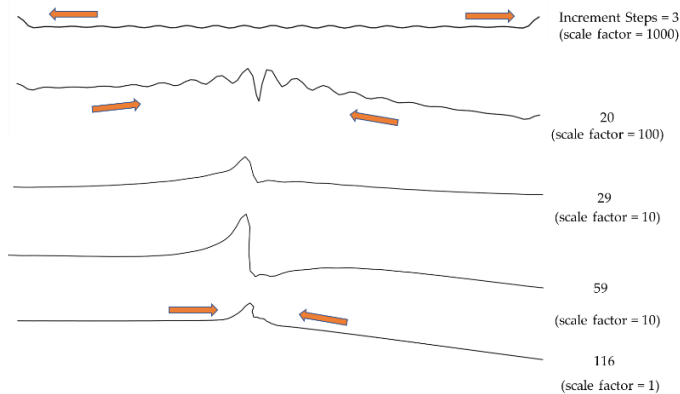


Figure 9 Shell (20 m at 30 mm) extreme fibre wavenumber change under bending.

At the third time increment of our simulations, the shell surface was adopted a wave-like shape. We selected this partial stage to run a curve-fitting manipulation using MATLAB, with the form of the sum of sinusoidal functions. The displacement function could not be validated by fewer than six parameters when including edge points, apparently due to the large deviation taking place near the end supports of the shell. We also observed that bending-buckling relies more heavily on the boundary conditions which contrast with the equivalent performance under axial compression. The significance of boundary conditions should be dealt with more in detail via complex displacement functions informed by some physical modelling.

In terms of circumferential curvature change, we used the cross section of the shell to scrutinise the ovalisation, for which we amplified the circumferential displacements shown in Figure 10, by a factor of 100 at steps 16 and 21. At step 16, the ovalisation emerged as a combined elliptical function involving multiple parameters, which proved that the simple ovalisation function may not be precise enough to represent the pre-buckling stage. At that point one sees an extremely rapid rate of change of local curvature, as demonstrated with increment steps 18 and 26. In those screenshots the inward dents are more noticeable than the bulge-shape outward displacement observed in the post-buckling process. Past increment step 26, the wavenumber maintained, and the failure became driven by the inward dents without any following bifurcation paths manifesting. The comparison between 20 m and 9 m shells of same wall thickness highlights the  $L/t$  ratio as weak parameter controlling of the buckle point location, whereas the position of the extension of buckled material depends highly on the supporting boundary conditions of the shells.

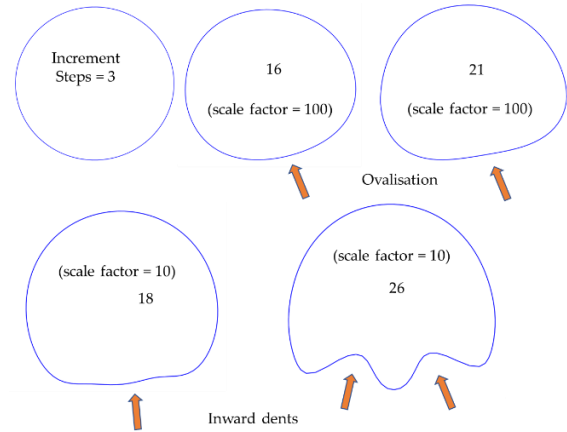
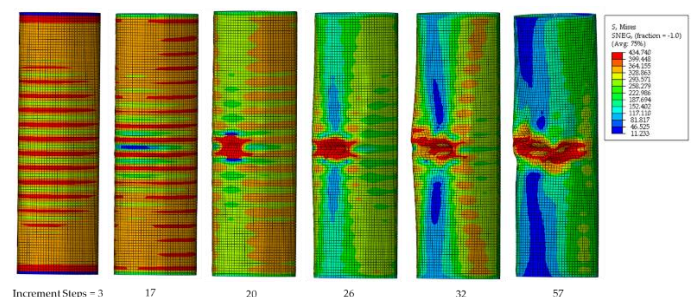
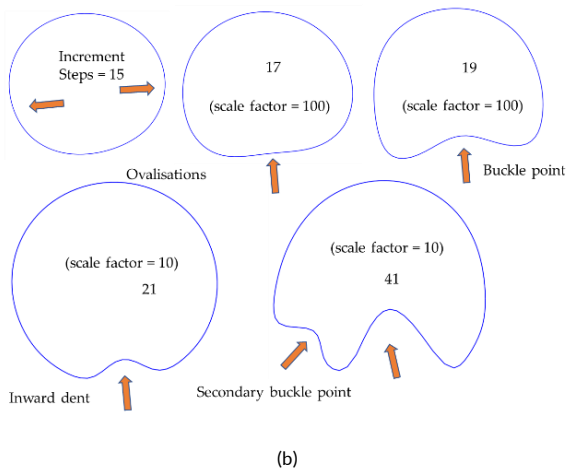


Figure 10 The cut-out view of the circumferential curvature change on 20 m at 30 mm shell under a bending moment.

Shell models with equivalent lengths and different thickness were selected for the analysis of the influence of the ratio  $R/t$ . Figure 11 shows a typical buckling sequence for the 20 m at 24 mm model. Notably, a similar type of buckling occurred on the shell of 24 mm. In that case, the buckle point emerged in the mid-span area, with more prominence than that observed on the 30 mm shell. The stress concentration led to one buckle point with a smaller adjacent area than the one of the shells shown in Figure 7. The single buckle point sustained for a longer period and the wavenumber progressions occurred in the late post-buckling stage, both circumferential and longitudinal. After the failure of the shell wall, less area was affected in the thin model than that of the thicker tube. The thinner shell buckling under bending also showed less wavenumber evolution, with a highly condensed buckle point emerging at the mid-span surface; this is due to the lower in-plane bending resistance capacity of thinner shells while the thicker shell showed better strain energy dissipation capacity. The loss of membrane effect in the buckled area resulted in the concentration of stress in its neighbourhood seemingly due to the large and rapid local curvature change on the shell surface. Figure 11 (b) illustrates the circumferential curvature change on the cross-section, including its ovalisation, recorded at increment steps 15 and 17. At increment step 19, we observed how the flattened region on the compression side abruptly buckled forming a single inward dent. This asymmetric buckling mode allowed more strain energy draining to the area and, after comprehensive evolutions, allow a secondary buckle point to emerge mainly due to the membrane effect loss in its adjacent area. These results reveal that the  $R/t$  ratio has significant effects on bending buckling sensitivity.



(a)



**Figure 11** (a) Shell (20 m at 24 mm) surface deformation and stress distribution under the pure bending moment; (b) The cut-out view of circumferential curvature change on the 20 m at 24 mm shell under bending moments.

#### 4.3 The Curvature - Energy Relations in Typical Buckling Induced Failure under Combined Loading Conditions

For combined loading we selected for scrutiny our models of 15 m and 12 m long with 24 mm wall thickness ( $R/t = 125$ ,  $L/R = 5$  and 4). Figure 12 illustrates the shell model performance including increment steps of a typical buckling progression. Figure 12 (a) illustrates how, under the combined loading condition, the in-plane strain energy emerged in the outline (as in axial compression scenarios) revealing longitudinal wavenumbers starting at step 54 that align with the pre-buckling shape function captured with a periodic trigonometric function. At increment step 61 and 100, during the transient buckling stage, a decrease of the longitudinal wavenumber resulted in mid-length strain energy concentration which balanced out with the increase of the circumferential wavenumber. This induced a buckle dent at the compression side with 2 wavenumbers above and 3 wavenumbers below the extreme fibre. From the increment step 168 to step 826 (post-buckling stage), the buckling gradually concentrated around one point and in turn lessened the in-plane strain energy in other shell parts. However, large displacements took place past this point, which activated the abrupt decrease of load bearing capacity that in turn limited the serviceability of the wind turbine tower.

According to Figure 12 (b), during the early stage of combined loading of the shell, changes of the inward circumferential curvature tended to accumulate on the compression side while a negligible outward curvature emerged on the tension side. At the increment step 100, three spots appeared along the half circle subject to compression, which anticipated how buckling would develop. Naturally, changes of curvature follow the distribution of strain energy. In this case, the circumferential curvature led to the ovalisation of the cross section already observed under pure bending effects. Under combined action, such distortion of the cross section maintains a significant contribution to buckling behaviour.

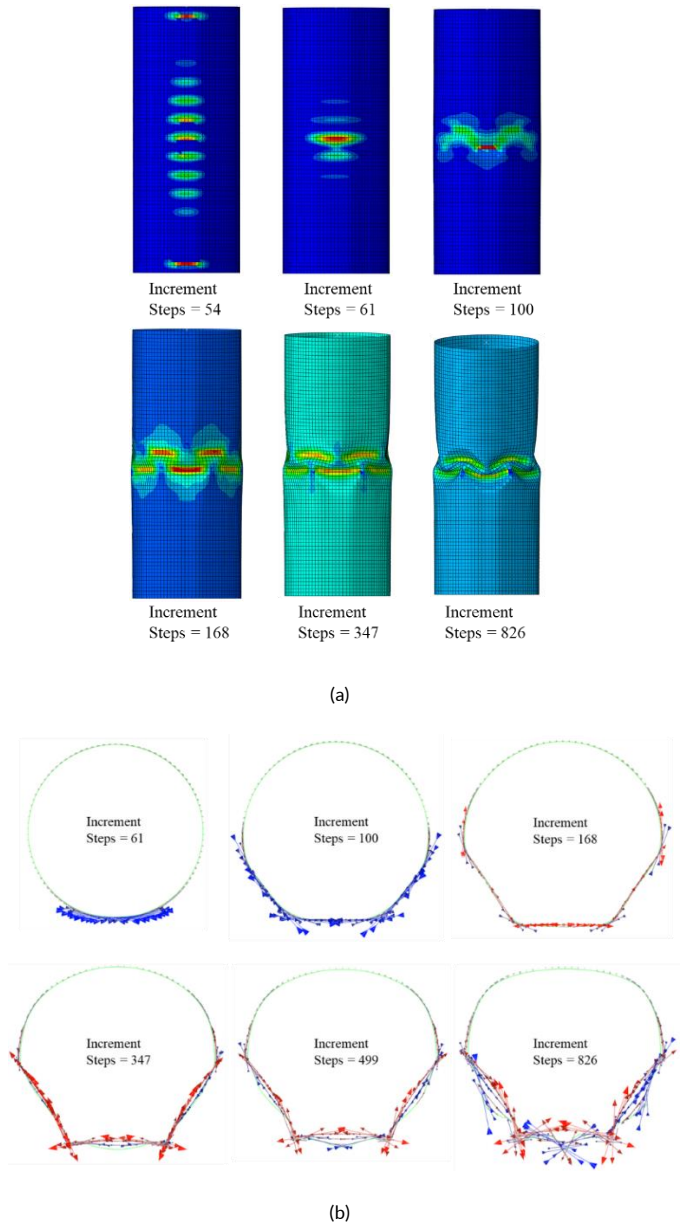


**Figure 12** (a) Shell (15 m at 24 mm) surface deformation and in-plane strain energy distribution under combined load; (b) The cut-out view of circumferential curvature changes.

Following, as the load incremented reached the interval of steps 168 to 347, the curvature redistribution characterised with four spots, associated to the buckling jumping mode. At the same time, the inward curvature changing tendency switched to its outward equivalent. The evolution of curvature largely associated to axial compression throughout the transient and post-buckling stages. As the process evolved to reach curvature increment steps 499 to step 826, the buckling jumping mode localised in relatively smaller sectors of the tower shell. Further to the evolution of curvature changes and in-plane strain energy distributions for varying shell length shown in Figure 13, the 12 m long shell model underwent fewer alternative curvature paths, most likely due to less material dissipation routes and stronger influence of its boundary conditions.



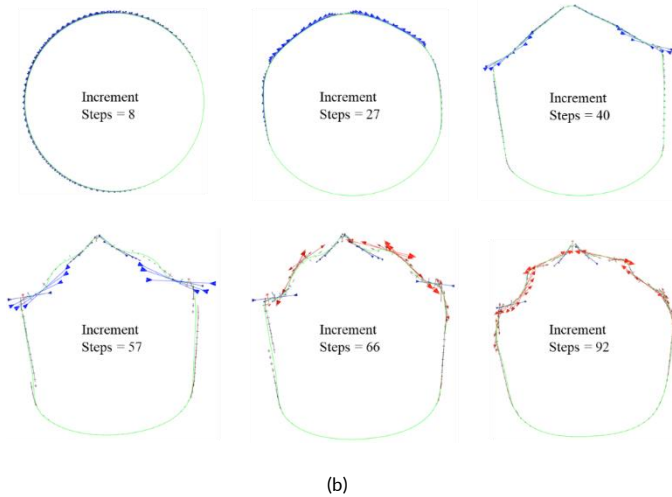
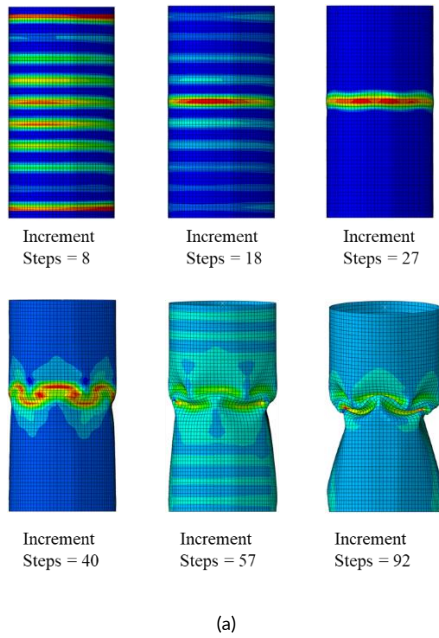


**Figure 13** (a) Shell (12 m at 24 mm) surface deformation and in-plane strain energy distribution under combined load; (b) The cut-out view of circumferential curvature changes on the 12 m with 24 mm wall thickness shell under combined load.

#### 4.4 Bending – Compression Ratios and Imperfections

To further investigate bending-axial interactions, we scrutinise the parametric study of 20 m shell models with five wall thicknesses. The combined loading was applied through a sequence batch of jobs in ABAQUS. The ratio of bending to compression was treated as non-dimensional unit progressively applied through magnitude increments of 0.05, covering the range 0 to 1.5. In this case, the buckling load factor refers to the theoretical result, which has been used in the knockdown factor study discussed in [12]. The best-fit curves of shells with different wall thicknesses have been drawn in Figure 14.

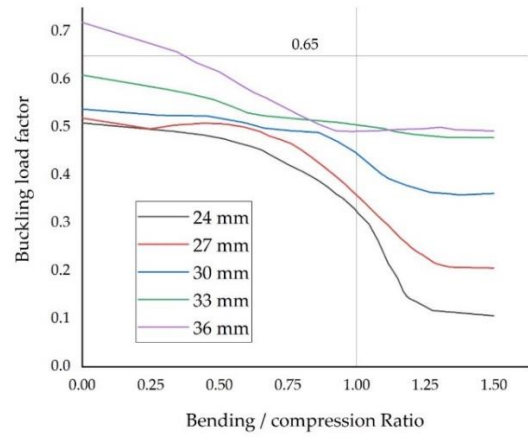


**Figure 14** The curves of the bending/compression ratio to buckling load factor for shell structure, under combined loading conditions with different wall thickness.

As illustrated in the figure, the reference value for axial compression is 0.65 [12], being the 36 mm shell the only one exceeding this lower bound, as a result of initial geometry imperfections. The thinnest 24 mm shell reported a rapid drop with the increase of the bending moment, suggesting that thinner shells have lower bearing capacity against bending effects. The 27 mm and 30 mm shells exhibited a similar trend under higher bending moment ratios, although with a milder decrease. Shells with thicker walls displayed better performance against the increased bending moment because of better energy dissipation routes and stronger interactions between longitudinal and circumferential curvatures.

The imperfection sensitivity under combined loading condition presented similar buckling performance than those seen for axial compression scenarios. Notwithstanding, buckling paths evolved faster due to shell imperfections that induced a rapid concentration of stress around weak areas; clearly, bending effects tended to accelerate such concentration. The buckling analysis under combined load considering initial imperfection thus establishes the most unfavourable conditions for a wind turbine tower in extreme wind events. It is therefore suggested that in this scenario, the obtained relations between bending and compression, and buckling behaviour investigations, are suggested to be used as enlightenment for future wind turbine tower design, either by means of energy methods or detailed numerical simulations.

#### 5 Conclusions

This paper addresses a series of 100 numerical shell models based on the prototype NREL 5MW wind turbine tower, underpinned by the known Riks Method for buckling analysis. It enables the scrutiny of shell elements under axial load, bending moment, and combined load. Within the proposed framework of curvature–energy analysis in pre-buckling, transient, and post-buckling stages, the numerical result unveils buckling-predictable changes of local surface curvature and energy flows with multiple longitudinal and circumferential wavenumbers taking place during the process. Wavenumbers and curvature changes induce the energy magnitude changes and buckling mode jumping: the circumferential wavelength has less influence on the axial compression buckling; other than the sensitivity of L/R ratio under axial compression, the R/t ratio and supporting boundary condition have significant effects on bending buckling sensitivity; the circumferential curvature changes stimulated by bending part have a remarkable

contribution to the buckling behaviour under axial-bending load. In combined loading conditions, the buckling behaviour sees a faster and more convergence result with higher bending moments, and the bending moments do more contributions to circumferential curvature changes and strain energy concentration, whereas the axial loads play more decisive role in longitudinal curvature evolution. The diversity of the final buckling mode largely determined by the variance of shell geometry, boundary conditions and compression–bending ratio.

## 6 Acknowledgement

The third author acknowledges with thanks the Alexander von Humboldt Stiftung for the continuous support to his research activities on High Performance Wind Energy Technology to enhance Sustainability and Resilience, as well as COST Action CA20109 MODENERLANDS for the support given in the field of the article.

## References

- [1] Ma, Y.; Martinez-Vazquez, P.; Baniotopoulos, C. (2019). *Wind turbine tower collapse cases: a historical overview*. Proceedings of the Institution of Civil Engineers - Structures and Buildings, 172, 547-555.
- [2] Lavassas, I.; Nikolaidis, G.; Zervas, P.; Efthimiou, E., Doudoumis, I.; Baniotopoulos, C. (2003). *Analysis and design of the prototype of a steel 1-MW wind turbine tower*. Engineering structures, 25, 1097-1106.
- [3] Van Es, S. H.; Gresnigt, A. M.; Vasilikis, D.; Karamanos, S. a. (2016). *Ultimate bending capacity of spiral-welded steel tubes-Part I: Experiments*. Thin-Walled Structures, 102, 286-304.
- [4] Vasilikis, D.; Karamanos, S. A.; Van Es, S. H. J.; Gresnigt, A. M. (2016). *Ultimate bending capacity of spiral-welded steel tubes - Part II: Predictions*. Thin-Walled Structures, 102, 305-319.
- [5] Karamanos, S. (2002). *Bending instabilities of elastic tubes*. International Journal of Solids and Structures, 39, 2059-2085.
- [6] Schneider, M. H. (1996). *Investigation of the stability of imperfect cylinders using structural models*. Engineering Structures, 18, 792-800.
- [7] Castro, S. G.; Zimmermann, R.; Arbelo, M. A.; Degenhardt, R. (2013). *Exploring the constancy of the global buckling load after a critical geometric imperfection level in thin-walled cylindrical shells for less conservative knock-down factors*. Thin-Walled Structures, 72, 76-87.
- [8] Dimopoulos, C. A.; Gantes, C. J. (2012). *Experimental investigation of buckling of wind turbine tower cylindrical shells with opening and stiffening under bending*. Thin-Walled Structures, 54, 140-155.
- [9] Wang, J.; Sadowski, A. J. (2020). *Elastic Imperfect Cylindrical Shells of Varying Length under Combined Axial Compression and Bending*. 146, 04020014.
- [10] Degenhardt, R.; Kling, A.; Zimmermann, R.; Odermann, F.; De Araújo, F. (2012). *Dealing with imperfection sensitivity of composite structures prone to buckling*. Advances in computational stability analysis. book edited by Safa Bozkurt Coskun, ISBN 978-953-51-0673-9.
- [11] Hornung, U.; Saal, H. (2002). *Buckling loads of tank shells with imperfections*. International Journal of Non-Linear Mechanics, 37, 605-621.
- [12] Peterson, J.; Seide, P.; Weingarten, V. (1968). *Buckling of thin-walled circular cylinders*. NASA Sp, 8007.
- [13] Von Karman, T.; Dunn, L. G.; Tsien, H. S. (1940). *The influence of curvature on the buckling characteristics of structures*. Journal of the Aeronautical Sciences, 7, 276-289.
- [14] Koiter, W. J. T. (1945). *On the stability of elastic equilibrium* (in Dutch).
- [15] Donnell, L. H.; Wan, C. C. (1950). *Effects of imperfections on buckling of thin cylinders and columns under axial compression*. Journal of Applied Mechanics, 73-83.
- [16] Hutchinson, J. W. (1968). *Buckling and Initial Postbuckling Behavior of Oval Cylindrical Shells Under Axial Compression*. Journal of Applied Mechanics, 35, 66-72.
- [17] Ma, L.; Wang, T. (2003). *Nonlinear bending and post-buckling of a functionally graded circular plate under mechanical and thermal loadings*. International Journal of Solids Structures, 40, 3311-3330.
- [18] Hu, H. T.; Yang, C. H.; Lin, F. M. (2006). *Buckling analyses of composite laminate skew plates with material nonlinearity*. Composites Part B: Engineering, 37, 26-36.
- [19] Fallah, A.; Aghdam, M. (2011). *Nonlinear free vibration and post-buckling analysis of functionally graded beams on nonlinear elastic foundation*. European Journal of Mechanics-A/Solids, 30, 571-583.
- [20] Hutchinson, J. (2016). *Buckling of spherical shells revisited*. Proceedings of the Royal Society A: Mathematical, Physical and Engineering Science, 472, 20160577.
- [21] Fitch, J.; James, R. (1968). *The buckling and post-buckling behavior of spherical caps under concentrated load*. 4, 421-446.
- [22] Wunderlich, W.; Albertin, (2002). *Buckling behaviour of imperfect spherical shells*. International Journal of Non-Linear Mechanics, 37, 589-604.
- [23] Von Karman, T.; Tsien, (1939). *The buckling of spherical shells by external pressure*. Journal of the Aeronautical Sciences, 7, 43-50.
- [24] Edlund, B. (2007). *Buckling of metallic shells: Buckling and postbuckling behaviour of isotropic shells, especially cylinders*. Structural Control and Health Monitoring, 14, 693-713.
- [25] Wu, J.; Zhu, J.; Dong, Y.; Zhang, Q. (2020). *Nonlinear stability analysis of steel cooling towers considering imperfection sensitivity*. Thin-Walled Structures, 146, 106448.
- [26] Hao, P.; Wang, B.; Tian, K.; Du, K.; Zhang, X. (2015). *Influence of imperfection distributions for cylindrical*

- stiffened shells with weld lands*. Thin-Walled Structures, 93, 177-187.
- [27] Khamlichi, A.; Bezzazi, M.; Limam, A. (2004). *Buckling of elastic cylindrical shells considering the effect of localized axisymmetric imperfections*. Thin-Walled Structures, 42, 1035-1047.
- [28] Von Karman, T.; Tsien, H. S. (1941). *The Buckling of Thin Cylindrical Shells Under Axial Compression*. Journal of the Aeronautical Sciences, 8, 303-312.
- [29] Donnell, L. H. (1934). *A new theory for the buckling of thin cylinders under axial compression and bending*. Transactions of The American Society of Mechanical Engineers, AER-56-12, 795-806.
- [30] Huang, H.; Han, Q. (2009). *Nonlinear elastic buckling and postbuckling of axially compressed functionally graded cylindrical shells*. International Journal of Mechanical Sciences, 51, 500-507.
- [31] Ma, Y.; Martinez-Vazquez, P.; Baniotopoulos, C. (2020). *Buckling Analysis for Wind Turbine Tower Design: Thrust Load versus Compression Load Based on Energy Method*. Energies. 13, 5302.
- [32] Hilbert, D.; Cohn-Vossen, S. (1999). *Geometry and the Imagination*, Chelsea Publishing (American Mathematical Society). ISBN-13 : 978-0821819982.
- [33] Calladine, C.; Sanders, J. (1984). *Theory of Shell Structures*. Journal of Applied Mechanics-transactions of The Asme - J Appl Mech, 51.
- [34] Teng, J. G.; Rotter, J. M. (2006). *Buckling of Thin Metal Shells*, CRC Press.
- [35] Gellin, S. (1980). *The plastic buckling of long cylindrical shells under pure bending*. International Journal of Solids and Structures, 16, 397-407.
- [36] Jonkman, J.; Butterfield, S.; Musial, W.; Scott, G. (2009). *Definition of a 5-MW reference wind turbine for offshore system development*. National Renewable Energy Lab. (NREL), Golden, CO (United States).
- [37] Abaqus, V. (2014). *6.14 Documentation*, Dassault Systemes Simulia Corporation.
- [38] Yamki, N.; Kodama, S. (1979). *Perturbation Analyses for the Postbuckling and Imperfection Sensitivity of Circular Cylindrical Shells under Torsion*. In *Theory of Shells* (Proceedings of 3rd IUTAM Symposium on Shell Theory), ed. W. T. Koiter and G. K. Mikhailov, 635-667.
- [39] Tafreshi, A. (2008). *Instability of delaminated composite cylindrical shells under combined axial compression and bending*. Composite Structures, 82, 422-433.
- [40] Brazier, L. G.; Southwell, R. V. (1927). *On the flexure of thin cylindrical shells and other "thin" sections*. 116, 104-114.